these resist systems, however, tend to be rounded due to the low T_g of the polymer and possible plasticization by the released aromatic compounds before volatilization. Recently, other workers have reported a similar type of resist system based upon polyethers containing alkoxypyrimidine units.[91] Resists made from these materials and triphenylsulfonium triflate exhibited sensitivites of 10 mJ/cm^2 upon irradiation at 250 nm. The products arising from acidolytic cleavage are pyrimidone and compounds containing both alkene and alcohol functionalities.

Conclusion

The aim of this review has been to examine one approach to the design of new resist chemistries for microlithographic applications. Chemical amplification processes utilize a single photochemical event that leads to a cascade of subsequent reactions effecting pattern differentiation within the parent material. The vast majority of materials that have been designed to date utilize a photochemically generated acid to catalyze subsequent cross-linking, deprotection, or depolymerization reactions. Significant efforts have been expended in the design of acid generator chemistries compatible with device processing environments. The most notable examples include the onium salts and nitrobenzyl esters. Additionally, the matrix resin must exhibit suitable characteristics with the most common materials being derived from hydroxyphenols.

Since the conception of chemical amplification mechanisms for microlithographic applications approximately one decade ago, increasing attention has been given to such processes in that they provide advantages in terms of sensitivity and contrast with minimal increase in process complexity. Additionally, a given chemistry may find application to more than one lithographic technology. The original work in chemically amplified resists has spawned many research efforts to define chemistries appropriate for matrix materials and photogenerators of catalysts, primarily strong acids. There continue to be many challenges in the areas of both fundamental and applied materials chemistry as well as process engineering to both understand and develop new chemically amplified resists for use with the future lithographic technologies.

(91) Inaki, Y.; Horito, H.; Matsumura, N.; Takemoto, K. *J. Photopolym. Sci. Technol.* **1990**, *3*, 417.

Articles

Oxovanadium(IV) Hydrogen Phosphate Hydrates: A Time-Resolved Neutron Powder Diffraction Study

Pedro Amorós,[†] Rafael Ibáñez,[†] Aurelio Beltrán,[†] Daniel Beltrán,*[,†] Amparo Fuertes,[‡] Pedro Gomez-Romero,[†,§] Eduardo Hernandez,[∥] and Juan Rodriguez-Carvajal[⊥]

UIBCM Departament de Química Inorgánica de la Universitat de Valencia, 46100-Burjassot, Valencia, Spain, the Instituto de Ciencia de Materiales de Barcelona, Spain, Departamento de Física Aplicada de la Universidad del Pais Vasco, Spain, and Institut Laue Langevin, Grenoble, France

Received July 19, 1990. Revised Manuscript Received January 24, 1991

Oxovanadium(IV) pyrophosphate, $(VO)_2P_2O_7$, is the catalytically active phase in the V–P–O system. It can be obtained by pyrolysis of any of the different hydrates of oxovanadium(IV) monohydrogen phosphate, $VO(HPO_4)\cdot yH_2O$ (y = 0.5, 1, 2 (α), 2 (β), 3, 4). The present neutron thermodiffractometric study shows unambiguously that, irrespective of the starting hydrate, the hemihydrate, $VO(HPO_4)\cdot 0.5H_2O$, always crystallizes before $(VO)_2P_2O_7$. The $VO(HPO_4)\cdot 0.5H_2O$ to $(VO)_2P_2O_7$ transformation is not a simple and straightforward process but involves an amorphous intermediate. The conversion of the different hydrates into $VO(HPO_4)\cdot 0.5H_2O$ requires more or less severe structural rearrangements, which, in turn, must affect the morphologic characteristics of the final catalyst.

Introduction

Oxovanadium(IV) hydrogen phosphate hydrates show a large structural diversity[1-5] that results in a very rich experimental magnetic behavior.[5-8] Moreover, they all are pyrolytic precursors of the oxovanadium(IV) pyro-

[†] UIBCM, Departament de Química Inorgánica, Universitat de Valencia, Doctor Moliner 50, 46100-Burjassot, Valencia, Spain.
* Author to whom correspondence should be addressed.
[‡] Instituto de Ciencia de Materiales de Barcelona, Martí i Franques s/n, 08028 Barcelona, Spain.
[§] Present address: Instituto de Ciencia de Materiales de Barcelona, Martí i Franques s/n, 08028 Barcelona, Spain.
[∥] Departamento de Física Aplicada, Universidad del Pais Vasco, Apdo. 644, Bilbao, Spain.
[⊥] Institut Laue-Langevin, 156 X 38042-Grenoble, France.

(1) Torardi, C. C.; Calabrese, J. C. *Inorg. Chem.* **1984**, *23*, 1308.
(2) Leonowicz, M. E.; Johnson, J. W.; Brody, J. F.; Shanon, H. F.; Newsam, J. M. *J. Solid State Chem.* **1985**, *56*, 370.
(3) Le Bail, A.; Ferey, G.; Amorós, P.; Beltrán, D.; Villeneuve, G. *J. Solid State Chem.* **1989**, *79*, 169.
(4) Le Bail, A.; Ferey, G.; Amorós, P.; Beltrán, D. *Eur. J. Solid State Inorg. Chem.* **1989**, *26*, 419.
(5) Beltrán, D.; Beltrán, A.; Amorós, P.; Ibáñez, R.; Martínez, E.; Le Bail, A.; Ferey, G.; Villeneuve, G. *Eur. J. Solid State Inorg. Chem.*, in press.
(6) Beltrán, D.; Amorós, P.; Ibáñez, R.; Martínez, E.; Beltrán, A.; Le Bail, A.; Ferey, G.; Villeneuve, G. *Solid State Ionics* **1989**, *32/33*, 57.

0897-4756/91/2803-0407$02.50/0

Table I. Reference Peaks Used for the Quantitative Analysis of the 3-D Plots[a]

phase	ref peak (*hkl*)	T_0	ΔT
$VO(HPO_4)\cdot 0.5H_2O$	101	291	$T > T_0$
α-$VO(HPO_4)\cdot 2H_2O$	100	300	$T > T_0$
β-$VO(HPO_4)\cdot 2H_2O$	011	300	$T > T_0$
$VO(HPO_4)\cdot 4H_2O$	002	300	$T > T_0$
$(VO)_2P_2O_7$	042	1000	$T < T_0$

[a] The percentage of each phase is calculated as the ratio $I_{hkl}(T)/I_{hkl}(T_0)$, where $I_{hkl}(T)$ and $I_{hkl}(T_0)$ represent the integrated intensity of the *hkl* reflection at T and T_0 (T_0 = temperature at which selected peaks reach their maximum intensity).

phosphate, $(VO)_2P_2O_7$, which has been recognized as the actually active phase in the catalytic preparation of maleic anhydride.[9,10] Although their chemistry has recently been studied in detail,[5,6,11] the mechanisms of the solid-state transformations leading from the different hydrates to $(VO)_2P_2O_7$ remain unexplained up to now.

The present investigation was undertaken to identify the intermediate phases in the course of the dehydration of the oxovanadium(IV) phosphates in order to achieve a better understanding of the transformations between the various structures. The conclusions of this work mainly rely on the results of a neutron thermodiffractometric (NTD) study. The use of time-resolved neutron powder diffractometry is particularly well suited to the study of thermally induced transformations in such hydrated materials since it provides simultaneous information about both the composition and structural characteristics of the solids.[12] The discussion of the NTD experiments has been developed in light of data from more conventional techniques, such as differential thermal analysis (DTA), thermogravimetric analysis (TGA), differential scanning calorimetry (DSC), and X-ray diffraction (XRD).

According to previous results,[11] the currently known vanadyl hydrogen phosphate hydrates could be grouped into three structural types, namely, type I ($VO(HPO_4)\cdot 0.5H_2O$), type II ($VO(HPO_4)\cdot yH_2O$, y = 1, 2 (α), and 3), type III ($VO(HPO_4)\cdot yH_2O$, y = 2 (β) and 4). Because of their structural peculiarities,[5] the understanding of the different dehydration processes leading to $(VO)_2P_2O_7$ might be relevant from the catalytic point of view.[9,10]

Experimental Section

Sample Preparation. The preparation of powder samples of the different oxovanadium(IV) hydrogen phosphate hydrates has been reported elsewhere.[11]

Neutron Thermodiffractometry. Neutron powder diffraction data were collected on the D1B two-axis diffractometer at the Laue Langevin Institute, using neutrons of wavelength 2.518 Å. The diffractometer has a 400-cell multidetector covering 80° in 2θ (in our case $12° \le 2\theta \le 92°$). The polycrystalline sample powder was packed into a cylindrical quartz tube (o.d. = 8 mm, h = 500 mm), held in a vanadium oven operating under vacuum ($P < 10^{-4}$ Torr). The temperature of the sample was increased at 48 K/h. Diffraction patterns were extracted every 3 min. An atmosphere of flowing nitrogen was used for all the samples. Correction for SiO_2 and equipment absorption was made systematically.

The diffraction patterns were analyzed numerically by least-squares fitting a Gaussian shape for each Bragg reflection and a first-order polynomial to the background.[13] The relative percentage of each phase was determined from the thermal evolution of the intensity of the well-isolated Bragg peaks listed in Table I. The background was averaged over a few cells in the adequate angular ranges where no reflection occurs along the dehydration processes. Data concerning the calculation of the percentages of each phase are summarized in Table I.

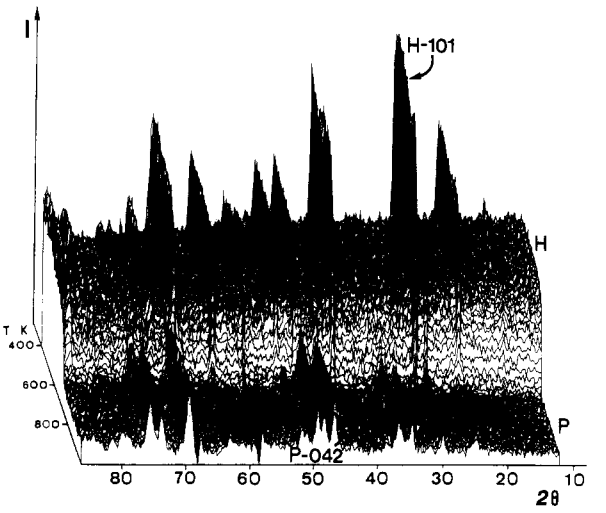

Figure 1. Neutron powder thermodiffractogram of the dehydration of $VO(HPO_4)\cdot 0.5H_2O$. H-101 and P-042 denote monitoring peaks from the hemihydrate (H) and pyrophosphate (P), respectively.

Because the background intensity (once corrected for SiO_2 and equipment absorption) is almost exclusively due to the incoherent scattering of the hydrogen atoms of the sample, the variation of this background intensity allowed us to determine the amount of hydrogen that remains in the solids at the different stages of the processes.

Other Techniques. Thermal analyses (TGA, DTA) were carried out using a Setaram B70 simultaneous thermobalance. Crucibles containing ca. 60 mg of sample were heated at 150 °C h^{-1} under a flowing N_2 atmosphere. Calcined Al_2O_3 was used as reference. Calorimetric measurements were performed using a Perkin-Elmer 7DSC in the temperature range $T_{room} \le T \le 400$ °C. Variations of sample size (25–100 mg) and/or heating rates (60–200 °C h^{-1}) do not result in significant changes in the thermoanalytical data. X-ray powder diffraction (XRD) patterns were obtained by means of a Siemens Kristalloflex 810 diffractometer using Cu Kα radiation and having the Pt peaks as standard. The apparatus is equipped with a variable-temperature device working from room temperature to ca. 1200 °C.

Results and Discussion

Dehydration of Type I Hydrate, $VO(HPO_4)\cdot 0.5H_2O$. As stated above, all the hydrogen phosphate hydrates yield pyrophosphate after pyrolysis. The structural link between the pyrophosphate and the hemihydrate is well established.[14-16] Thus, it might reasonably be assumed that the mechanism of the $VO(HPO_4)\cdot 0.5H_2O$ to $(VO)_2P_2O_7$ solid-state transformation is comparatively simple and probably involved in the course of the dehydration of the higher hydrates.[17]

Figure 1 shows a pseudo-3-D diagram ($I = f(\theta,T)$) rep-

(7) Villeneuve, G.; Amorós, P.; Beltrán, D.; Drillon, M. *Organic and Inorganic Low Dimensional Crystalline Materials*; Delhaes, P., Drillon, M. Eds.; NATO ASI Series; Plenum Press: New York, 1987; Vol. B168, p 417.
(8) Wrobleski, J. T. *Inorg. Chem.* **1988**, *27*, 946.
(9) Centi, G.; Trifiro, F.; Ebner, J. R.; Franchetti, V. M. *Chem. Rev.* **1988**, *88*, 55.
(10) Hodnett, L. *Catal. Rev.-Sci. Eng.* **1985**, *27*, 373.
(11) Amorós, P.; Ibáñez, R.; Martínez, E.; Beltrán, A.; Beltrán, D.; Villeneuve, G. *Mater. Res. Bull.* **1989**, *24*, 1347.
(12) Pannetier, J. *Chem. Scr.* **1985**, *26A*, 131.
(13) Wolfers, P. INTGR, unpublished computer program, 1975.
(14) Bordes, E.; Courtine, P.; Johnson, J. W. *J. Solid State Chem.* **1984**, *55*, 270.
(15) Johnson, J. W.; Johnston, D. C.; Jacobson, A. J.; Brody, J. F. *J. Am. Chem. Soc.* **1984**, *106*, 8123.
(16) Gorbunova, Y.; Linde, S. A. *Dokl. Akad. Nauk. SSSR* **1979**, *245*, 584.
(17) This is in spite of the fact that the hemihydrate stabilization is not detected in thermoanalytical (DTA, TGA) experiments with higher hydrates (see ref 11).

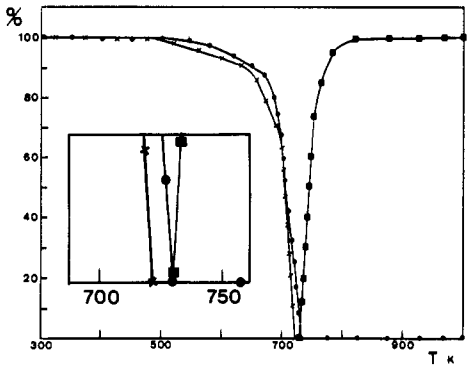

Figure 2. Thermal evolution of the integrated intensities of the monitoring peaks, H-101 (×) and P-042 (■). Background (●).

resenting the thermal evolution of the neutron powder diffractogram of $VO(HPO_4)\cdot 0.5H_2O$ in the range 292–1000 K. As can be noted, the background level decreases slowly from ca. 500 to 650 K and then more rapidly until 730 K. At this last temperature, the only crystalline phase present is $(VO)_2P_2O_7$.[16] Figure 2 represents a quantitative analysis of the 3-D diagram in terms of the background level and the fraction of each phase present during the dehydration process. From it, the following remarks can be made: (1) The hemihydrate is stable under N_2 (1 atm) up to ca. 510 K. The position of its 101 peak remains unchanged (2θ = 32.38°) while it exists. The width at half-height (fwhm) of this peak also remains practically constant up to 705 K. (2) Between 510 and 650 K a slow decrease of the background level takes place, indicating the onset of the dehydration process. At the same time the intensity I_{101} of $VO(HPO_4)\cdot 0.5H_2O$ decreases ca. 10%. (3) The condensation reaction occurs mainly in the range 650–722 K, coinciding with a steep decrease of the background level to a minimum at 730 K. The structural breakdown of the hemihydrate is completed slightly before the total dehydration: the 101 peak of the hemihydrate—whose widening started at 705 K—disappears at 722 K and there is no peak in the range 722–730 K. (4) The intensity of the reflections due to $(VO)_2P_2O_7$, the only ones present above 730 K, increases rapidly to reach its maximum value at 800 K and then remains constant up to 1000 K.

The total weight loss in the process, as measured by the background level decrease, represents an 11.5% of the starting sample. This value fits in well with the equation

$$2VO(HPO_4)\cdot 0.5H_2O \rightarrow (VO)_2P_2O_7 + 2H_2O$$

i.e., it corresponds to the removal of one water molecule shared by two vanadium atoms plus that of one more water molecule coming from the condensation of two $[HPO_4]$ groups.

It is worthwhile to emphasize here that both crystalline phases do not coexist at any temperature during the dehydration: the reaction does not occur in a single stage but involves the formation of a reactive amorphous intermediate phase. The formation of this intermediate or $(VO)_2P_2O_7$ *precursor* phase is relevant because it occurs during all the pyrolytic processes considered in this work (see below).

In light of the NTD analysis (Figure 2), the *precursor* phase is formed after elimination of ca. 0.8 water molecule/vanadium atom (from the background level at 722 K, just when no peak of $VO(HPO_4)\cdot 0.5H_2O$ is observed), a result that nicely agrees with our previous observations based on thermoanalytical (DTA, TGA) techniques.[11] Thus, our previous hypothesis on the existence of a metastable intermediate in the course of the progressive joining of the $(VOHPO_4)_\infty$ sheets[11] finds now a strong support in

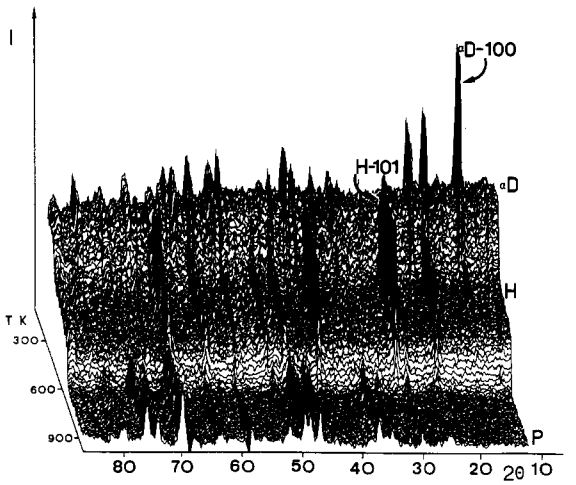

Figure 3. Neutron powder thermodiffractogram of the dehydration of α-$VO(HPO_4)\cdot 2H_2O$. αD-100, H-101, and P-042 denote monitoring peaks from the α-dihydrate (αD), the hemihydrate (H), and pyrophosphate (P), respectively.

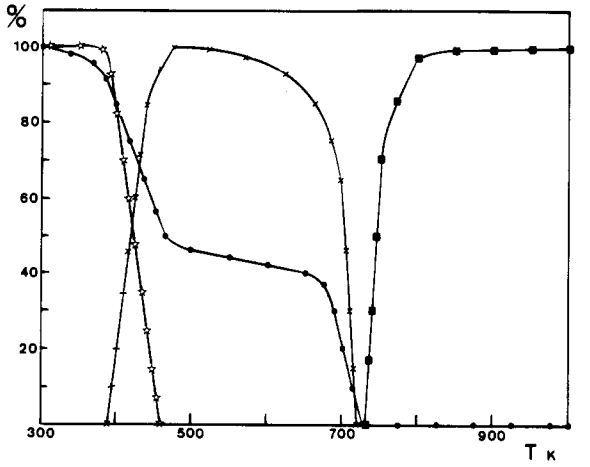

Figure 4. Thermal evolution of the integrated intensities of the monitoring peaks, αD-100 (☆), H-101 (×) and P-042 (■). Background (●).

the NTD experiment. We will return to this aspect later on.

Dehydration of Type II Hydrates, $VO(HPO_4)\cdot yH_2O$ (y = 1, 2 (α), 3). Dealing with this series, the fact that both the trihydrate and the monohydrate easily yield the α-dihydrate[11] suggested to us the choice of α-$VO(HPO_4)\cdot 2H_2O$ as the model for NTD experiments on this structural type.

The $I = f(\theta,T)$ diagram ($300 \leq T \leq 1000$ K) and its quantitative analysis are shown in Figures 3 and 4, respectively. The general features of the dehydration process can be summarized as follows: (1) Although the onset of the dehydration occurs between 300 and 375 K, as indicated by a slight decrease (ca. 5%) of the background level, the intensity I_{100} of the reference peak of α-$VO(HPO_4)\cdot 2H_2O$ remains practically unaltered up to 375 K. (2) The dehydration process progresses steeply between 375 and 470 K. The I_{100} of α-$VO(HPO_4)\cdot 2H_2O$ decreases sharply until disappearing at 460 K. Simultaneously, the Bragg peaks due to $VO(HPO_4)\cdot 0.5H_2O$ grow rapidly from 390 to 475 K, where a maximum intensity of its monitoring peak (101) is reached. Therefore, both phases coexist in the range 390–460 K. (3) During this process, it is to be noted that both the position (2θ = 19.10°) and the fwhm of the 100 peak of α-dihydrate remain constant until 435 K. This peak shifts then to a slightly lower angular value (2θ = 19.03°), while its fwhm increases markedly. (4) Once the

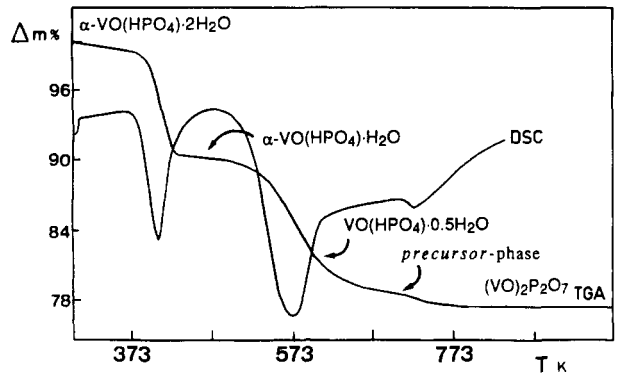

Figure 5. TGA-DSC plots for α-$VO(HPO_4)\cdot 2H_2O$.

hemihydrate is formed (ca. 475 K), the NTD experimental behavior practically reproduces that described in the previous section.

The NTD experiment thus proves unambiguously the involvement of $VO(HPO_4)\cdot 0.5H_2O$ in the dehydration mechanism of higher hydrates. As stated above, this hypothesis was based on structural qualitative considerations but it was not clearly confirmed by previous results.[11] So, it seemed to us appropriate to reexamine our previous thermoanalytical data with the aid of another conventional technique, differential scanning calorimetry (DSC). Figure 5 includes both the TGA and DSC curves corresponding to α-$VO(HPO_4)\cdot 2H_2O$. As can be noted, there is no plateau in the TGA curve that indicates the stabilization of the hemihydrate during the reaction. The DSC curve, however, clearly shows three endothermic effects that can be attributed (by comparison with the TGA curve) to the formation of the monohydrate, the hemihydrate and the above so-called *precursor* phase. The hemihydrate appears here as a highly reactive intermediate that rapidly evolves to the *precursor*. Its detection, nevertheless, has been possible with the NTD experiment. In any case, the different kinetics of this NTD experiment with regard to those performed by more conventional techniques is now evident. The observed discrepancies (no detection of the monohydrate and, on the contrary, a long temperature range in which the hemihydrate is stabilized in the NTD experiment) are very likely related to differences in the sample size and ventilation and in the geometric characteristics of the holders.[18,19]

These considerations show us again how careful attention must be paid when working with a given series of hydrates: results coming from only one type of dynamic technique—regardless of its potential power—may easily be misunderstood. In fact, as shown in Figure 6, a new set of room-temperature XRD experiments, made on samples previously heated at the specified temperature, has now allowed us to identify all of the crystalline intermediates in the dehydration of α-$VO(HPO_4)\cdot 2H_2O$.

Given that the monohydrate takes up water reversibly (at room temperature) to yield α-$VO(HPO_4)\cdot 2H_2O$, which is also formed by gentle heating of the trihydrate, it seems reasonable to assume that the main features of the dehydration process are common for all three hydrates in this series. These main features are, in short, the formation of $VO(HPO_4)\cdot 0.5H_2O$ and the *precursor* phase as pyrolytic intermediates of $(VO)_2P_2O_7$.

Dehydration of Type III Hydrates, $VO(HPO_4)\cdot yH_2O$ (y = 2 (β), 4). The general features of the dehydration of β-$VO(HPO_4)\cdot 2H_2O$ and $VO(HPO_4)\cdot 4H_2O$ are presented in Figures 7 and 8, respectively. Quantitative analyses of these pseudo 3-D plots lead to Figures 9 and 10, respectively.

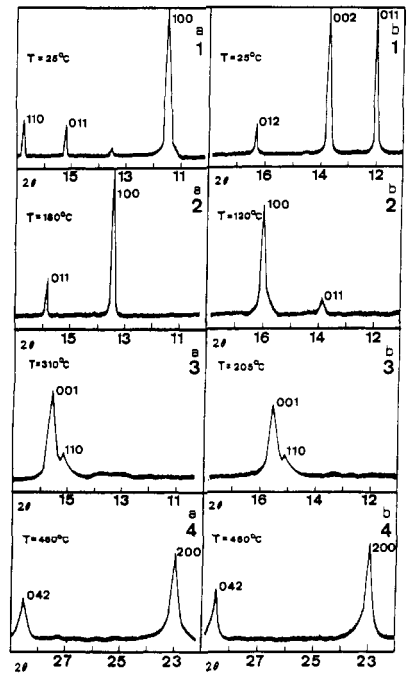

Figure 6. X-ray powder diffraction patterns of samples heated at the specified temperature. Series a corresponds to samples coming from α-$VO(HPO_4)\cdot 2H_2O$ (1 = α-$VO(HPO_4)\cdot 2H_2O$, 2 = $VO(HPO_4)\cdot H_2O$, 3 = $VO(HPO_4)\cdot 0.5H_2O$, and 4 = $(VO)_2P_2O_7$). Series b correspond to samples coming from $VO(HPO_4)\cdot 4H_2O$ (1 = $VO(HPO_4)\cdot 4H_2O$, 2 = β-$VO(HPO_4)\cdot 2H_2O$, 3 = $VO(HPO_4)\cdot 0.5H_2O$, and 4 = $(VO)_2P_2O_7$).

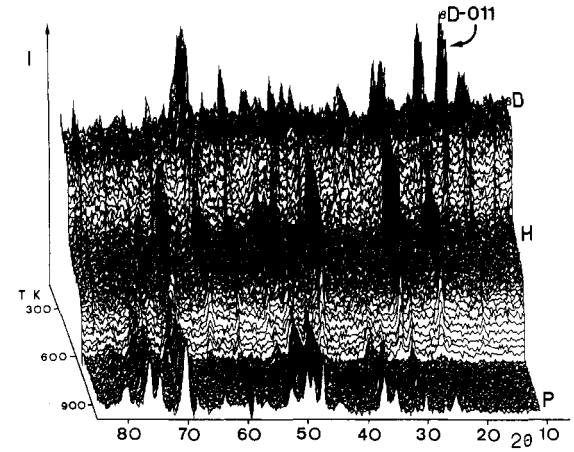

Figure 7. Neutron powder thermodiffractogram of the dehydration of β-$VO(HPO_4)\cdot 2H_2O$. βD-011, H-101, and P-042 denote monitoring peaks from the β-dihydrate (βD), the hemihydrate (H), and pyrophosphate (P), respectively.

As shown in Figure 7, the dehydration process of β-$VO(HPO_4)\cdot 2H_2O$, like that of α-$VO(HPO_4)\cdot 2H_2O$, involves two stages. Two sharp drops in the background level are observed at 420–475 and 650–720 K. According to the analysis in Figure 9, we can summarize this process as follows: (1) In the range 300–400 K a slight decrease of the background level (ca. 7%) takes place while the intensity of the 011 reflection of the β-dihydrate (2θ = 22.50°) stays constant. At 425 K the peak 011 of the β-dihydrate collapses completely, while at 410 K the hemihydrate appears and crystallizes rapidly, as monitored with its 101 reflection (whose maximum intensity is attained at ca. 500 K). Thus, the range of coexistence of

(18) Logvinenko, J.; Paulik, J.; Paulik, F. J. *Therm. Anal.* **1976**, *10*, 265.
(19) Paulik, J.; Paulik, F.; Logvinenko, V. J. *Therm. Anal.* **1976**, *10*, 123.

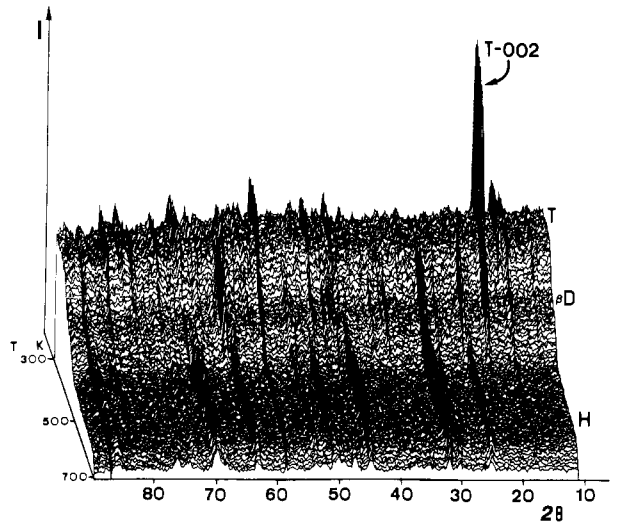

Figure 8. Neutron powder thermodiffractogram of the dehydration of $VO(HPO_4)\cdot 4H_2O$. T-002, βD-011, and H-101 denote monitoring peaks from the tetrahydrate (T), the β-dihydrate (βD), and the hemihydrate (H), respectively.

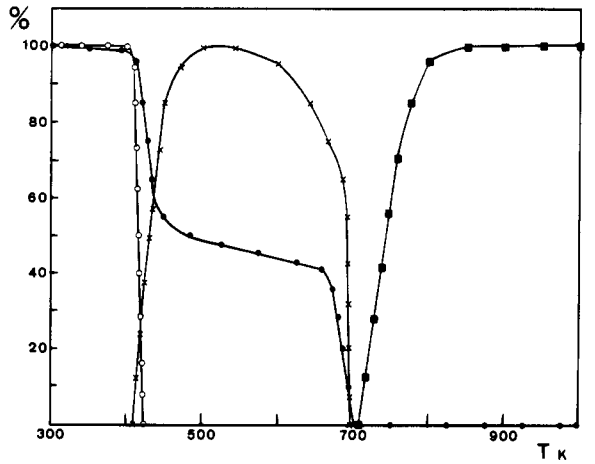

Figure 9. Thermal evolution of the integrated intensities of the monitoring peaks, βD-011 (○), H-101 (×) and P-042 (■). Background (●).

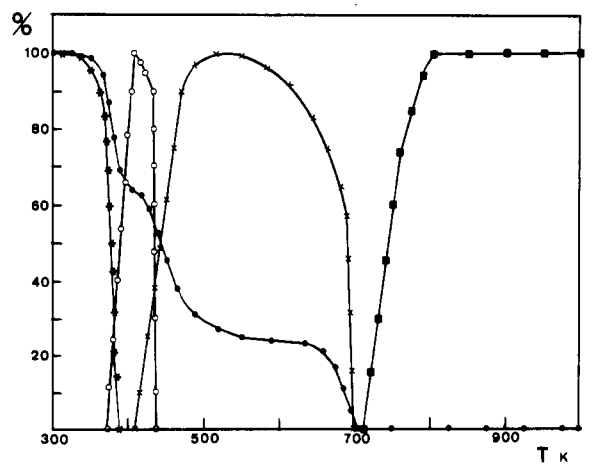

Figure 10. Thermal evolution of the integrated intensities of the monitoring peaks, T-002 (*), βD-011 (■), H-101 (×), and P-042 (■). Background (●).

these phases (15 K) is narrower than that observed in the α-dihydrate case (70 K). (2) The temperature of this first dehydration step is higher than for the α case, as should be expected, since the α-phase contains uncoordinated water while the β-phase does not. (3) After the hemihydrate formation (ca. 500 K), the second dehydration step, leading to $(VO)_2P_2O_7$, is practically identical with the one observed for the α phase.

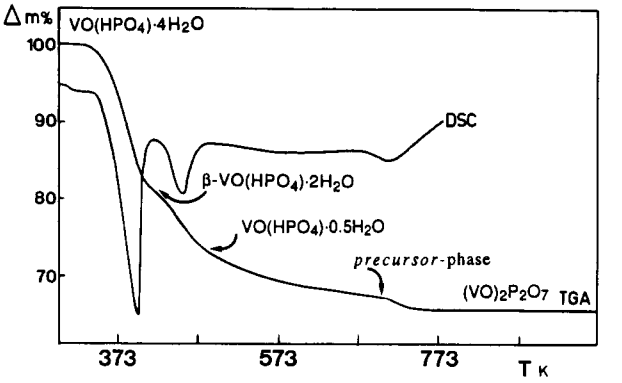

Figure 11. TGA-DSC plots for $VO(HPO_4)\cdot 4H_2O$.

On the other hand, as shown in Figures 8 and 10, the two additional water molecules of the tetrahydrate only introduce a new step in the dehydration process. This, which begins now at lower temperature (ca. 340 K), can be summarized as follows: (1) At 345 K, I_{002} (the intensity of the reference peak of the $VO(HPO_4)\cdot 4H_2O$) begins decreasing faster than the background level. Near 400 K the first dehydration step, converting the tetrahydrate into the β-dihydrate, is completed. Peak 002 of $VO(HPO_4)\cdot 4H_2O$ collapses rapidly, dissappearing completely at 393 K. Peak 011 of β-$VO(HPO_4)\cdot 2H_2O$ appears at 375 K and also grows rapidly. It reaches at 400 K 73% of its maximum intensity, which is attained at 419 K. Thus, the β-dihydrate coexists with the tetrahydrate during a relatively narrow range of 18 K. (2) During this step, β-$VO(HPO_4)\cdot 2H_2O$ predominates only in a narrow range of temperature (there is no plateau associated with β-$VO(HPO_4)\cdot 2H_2O$ either in the background level or in I_{011}) before decomposing. (3) The second dehydration step (ca. 410–450 K) leads again from the β-phase to the hemihydrate, and from there the behavior of the system can be described as above.

In short, in accordance with the NTD results, the global dehydration process can be schematized as

$$VO(HPO_4)\cdot 4H_2O \rightarrow (1-x)VO(HPO_4)\cdot 4H_2O + x(\beta\text{-}VO(HPO_4)\cdot 2H_2O) \dashrightarrow \beta\text{-}VO(HPO_4)\cdot 2H_2O \rightarrow (1-x)\beta\text{-}VO(HPO_4)\cdot 2H_2O + xVO(HPO_4)\cdot 0.5H_2O \rightarrow VO(HPO_4)\cdot 0.5H_2O \rightarrow precursor \rightarrow \tfrac{1}{2}(VO)_2P_2O_7 + \tfrac{1}{2}H_2O$$

a scheme that encompasses the formation and dehydration of the β phase as a part.

Following our analysis of the α-phase, we have performed a new DSC experiment with the tetrahydrate in order to clarify our previous thermoanalytical data.[11] DSC–TGA curves corresponding to $VO(HPO_4)\cdot 4H_2O$ are presented in Figure 11. As can be noted, the DSC curve displays only three endothermic effects, which can be associated through the TGA curve to the formation of β-$VO(HPO_4)\cdot 2H_2O$, $VO(HPO_4)\cdot 0.5H_2O$, and the *precursor* phase. Again, the DSC experiment allows us to detect the previously missing hemihydrate and confirms the kinetic differences arising from different experimental procedures. Otherwise, the expected lack of the monohydrate is consistent with the different behavior of the two polymorphs, α and β, of the dihydrate, differences that have to be explained on the basis of their structural characteristics.

Concluding Remarks

As stated above, our aim in this study was to progress in the understanding of the solid-state transformations

between the various structures of the vanadyl hydrogen phosphate hydrates and of these structures into that of $(VO)_2P_2O_7$. Having established the steps involved in the different dehydration processes, it seems possible to advance reasonable proposals concerning the mechanisms of such transformations.

As we have emphasized, regardless of the starting hydrate, all the pyrolytic processes studied here involve, as expected, the hemihydrate as the last crystalline phase appearing before the pyrophosphate formation. An important additional observation, however, is the systematic detection of the amorphous *precursor* reactive phase after elimination of ca. 60% of the condensation water coming from the hydrogen phosphate groups. Because of its ubiquity, this two-step process [$VO(HPO_4)\cdot 0.5H_2O \rightarrow$ *precursor* + ca. $0.8H_2O \rightarrow {}^1/_2(VO)_2P_2O_7 + H_2O$] plays an essential role in the routes to pyrophosphate.

Although the formation of the metastable *precursor* has not been observed up to now, some authors—on the basis of structural arguments—have suggested that the transformation of $VO(HPO_4)\cdot 0.5H_2O$ into $(VO)_2P_2O_7$ might occur topotactically.[14,15] Both structures are lamellar, and the step from $VO(HPO_4)\cdot 0.5H_2O$[1,2] to $(VO)_2P_2O_7$[16] would formally require (a) the elimination of the coordinated water molecules (shared by two vanadium atoms), and (b) the joining of the resulting $[VO(HPO_4)]_\infty$ sheets. This last step would involve both the linking two-by-two of $[VO_6]$ octahedra of adjacent layers to give double chains along the *b* direction (which should satisfy again vanadium six-coordination), and the condensation of $[HPO_4]$ tetrahedra to give the bridged $[O_3P-O-PO_3]$ pyrophosphate entities.[11,15] A closer look at the available data indicates that the elimination of coordinated water and the beginning of the layer uniting are concerted processes, but the thermal data (and NTD results) associated with the appearance of the *precursor* show that the condensation of $[HPO_4]$ groups occurs in stepwise fashion.

Moreover, the independence of the precursor formation with respect to the starting material suggests that this effect is due to the very nature of the condensation process. In reality, given the structural features of $VO(HPO_4)\cdot 0.5H_2O$,[1,2] while a single contraction along the 001 axis would allow the formation of the oxovanadium double chains, a concerted displacement of the layers along the [110] direction is needed in order to collapse the $[HPO_4]$ groups into $[P_2O_7]$ entities. While activation of this simple movement would require very little energy, its total synchronism might easily be disrupted by any local defect. These defects would imply the permanence of the linking of $[HPO_4]$ groups to three $[VO_6]$ octahedra in such as way that their OH units would remain misdirected to connect to other $[HPO_4]$ entities. In this way, we might understand both the amorphous character of the *precursor* and the fact that its conversion into $(VO)_2P_2O_7$ goes to completion only at high temperatures. In fact, a new mechanism—involving atomic diffusion (and, consequently, a relatively high activation energy)—would be needed to complete the water removal. Indirect evidence in this sense is provided by earlier observations of the catalytic role of small amounts of protonic species in the condensation of other pyrophosphates.[20] An analogous trapped defect mechanism might be argued to explain the previously reported formation of an intermediate phase in the course of the condensation of $VO(H_2PO_4)_2$ to $VO(PO_3)_2$.[11] In this case, a concerted twist of the $[VO_6]$ octahedra is required to connect $[H_2PO_4^-]$ pseudotetrahedral entities into the dimeric edge shared $[P_2O_6]$ groups.[21]

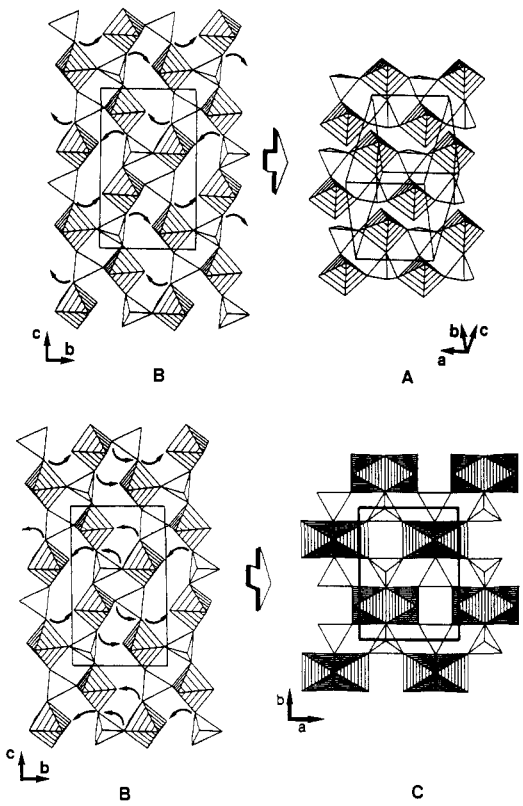

Figure 12. One possible topochemical path connecting $VO(HPO_4)\cdot 4H_2O$ (A), β-$VO(HPO_4)\cdot 2H_2O$ (B), and $VO(HPO_4)\cdot 0.5H_2O$ (C). It can be noted that the relative disposition of the vanadyl groups is maintained after each step.

This mechanism would very likely be less energy-expending than that suggested in ref 1. In fact, in that case phosphate groups are inadequately oriented in order to condense into pyrophosphate entities.

As long as the nature of the final two-step transformation is not affected by the starting hydrate, what confers specificity to each pyrolytic process has to be the character of the reactions leading to $VO(HPO_4)\cdot 0.5H_2O$. In this sense, there are reasonable pathways allowing the structural modifications required for the transformations tetrahydrate → β-dihydrate → hemihydrate to occur topochemically (according to Rao's definition[22]). One such possible mechanism has been schematized in Figure 12. The step from $VO(HPO_4)\cdot 4H_2O$[2,5] to β-$VO(HPO_4)\cdot 2H_2O$[3,5] leaves largely unaffected both the nature of V(IV) coordination polyhedra and the arrangement of the vanadium to oxygen double bonds (i.e., the vanadyl groups), which remain quasi-perpendicular to the propagation direction of the chains (tetrahydrate) or layers (β-dihydrate). Although the subsequent dehydration step (leading to the hemihydrate) seems to be just a little more involved because of the changes in the coordination polyhedron of V(IV), it must be stressed that the relative disposition of the [V=O] groups (as well as the lamellar array) is also essentially maintained. On the contrary, the conversion α-$VO(HPO_4)\cdot 2H_2O \rightarrow VO(HPO_4)\cdot H_2O \rightarrow VO(HPO_4)\cdot 0.5H_2O$ as a whole is highly hindered. Thus, whereas the reversible reaction α-$VO(HPO_4)\cdot 2H_2O \rightarrow VO(HPO_4)\cdot H_2O$ can be thought of as strictly topotactic (Figure 13), to bring

(20) Van Wazer, J. R. *Phosphorus and its Compounds*; Interscience Publishers: London, 1958, Vol I.

(21) Erragh, A. Thèse d'Etat, Université de Bordeaux I, France, 1986. Erragh, A.; Darriet, J.; Villeneuve, G.; Chaminade, J. P.; *Phys. Status Solidi*, submitted.

(22) Rao, C. N. R.; Gopalakrishnan, *New directions in solid state chemistry*; Cambridge University Press: Cambridge, 1986.

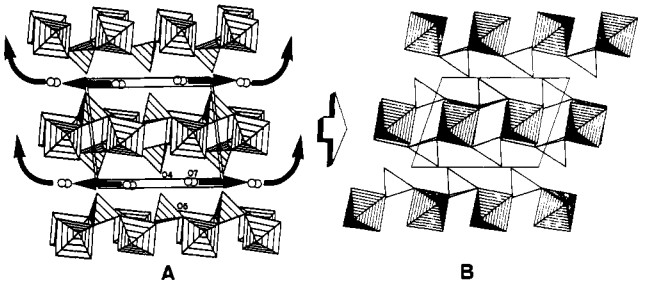

Figure 13. Possible mechanistic scheme for the topotactic transformation from α-$VO(HPO_4)\cdot 2H_2O$ (A) to $VO(HPO_4)\cdot H_2O$ (B).

the vanadyl groups out of the layer planes on which they lie in the monohydrate and put them in the quasi-perpendicular disposition they have in the hemihydrate must imply a full structural breakdown of the initial bonding network. In practice, as pointed out above, it results in the comparatively high temperature required for this transition. It may be similarly understood that, when performing NTD experiments, the range of temperatures in which the formation of $VO(HPO_4)\cdot 0.5H_2O$ goes to completion is significantly larger for the α phase than for the β phase.

Moreover, the reversible character of the α-$VO(HPO_4)\cdot 2H_2O \leftrightarrow VO(HPO_4)\cdot H_2O$ process implies that both the temperature of elimination of this first water molecule and the existence range of the monohydrate would be highly dependent on the partial pressure of water vapor in the reaction vessel. This fact may well account for the nonobservance of the monohydrate in the respective NTD experiment. On the contrary, the dehydration processes involving type III phosphates are clearly irreversible and consequently independent of this parameter.

In any case, according to the TGA-DSC data, the in situ formation of $VO(HPO_4)\cdot 0.5H_2O$ (from a higher hydrate) enhances significantly its reactivity.[23] From the data presented above, it seems evident that this different reactivity must be due to differences in crystallinity and morphologic characteristics of the solids, which, in turn, should be very likely related to the nature of the structural changes required for $VO(HPO_4)\cdot 0.5H_2O$ formation. In short, any phase transformation that involve hydrates belonging to different structural types will be hindered. As the topological modifications required become more drastic (i.e., type II → type I > type III → type I),[5] (a) the hemihydrate formation will require a higher temperature, (b) it will consist of smaller particles of lower crystallinity, and (c) it will react more easily to yield the amorphous *precursor* phase.

As might be expected, preliminary scanning electron microscopy (SEM) results show that the morphological characteristics of the final pyrophosphate are highly dependent on the starting hydrate. Because of the relevance of this factor from the catalytic point of view, a more detailed surface characterization study is currently in progress.

Acknowledgment. The Institut Max von Laue-Paul Langevin, Grenoble, is thanked for the use of the neutron powder diffraction instrument. We thank the DGICYT for partial financial support.

Registry No. $VO(HPO_4)\cdot 0.5H_2O$, 93280-40-1; $VO(HPO_4)\cdot H_2O$, 126122-85-8; $VO(HPO_4)\cdot 2H_2O$, 118654-93-6; $VO(HPO_4)\cdot 3H_2O$, 97701-41-2; $VO(HPO_4)\cdot 4H_2O$, 96241-67-7; $(VO_2)P_2O_7$, 58834-75-6.

(23) For heating rates of 150 °C/h under a flowing N_2 atmosphere, dehydration of crystalline $VO(HPO_4)\cdot 0.5H_2O$ begins at 430 °C, whereas it occurs at ca. 205 or 330 °C when the hemihydrate comes from β-dihydrate or α-dihydrate, respectively.

Selective Incorporation and Aggregation of Pyrene in a Segmented Poly(urethane urea) Film As Revealed by Picosecond Total Internal Reflection Fluorescence Spectroscopy

Masatoshi Yanagimachi, Minoru Toriumi,* and Hiroshi Masuhara*

Microphotoconversion Project, ERATO, Research Development Corporation of Japan, 15 Morimotocho, Shimogamo, Sakyo-ku, Kyoto 606, Japan

Received August 29, 1990. Revised Manuscript Received March 15, 1991

Fluorescence spectra and dynamics of pyrene doped in segmented poly(urethane urea) (SPUU, copolymer of toluene-2,4-diisocyanate (TDI) and poly(propylene oxide) (PPO)) films are studied by means of time-resolved total internal reflection (TIR) fluorescence spectroscopy. The differences in the environmental polarity and aggregates of pyrene between the surface layer (ca. 52 nm) and bulk layer (>0.68 μm) in the SPUU films are elucidated. The present results on the fluorescence characteristics and dynamics strongly indicate that pyrene molecules in the surface layer of the film are located in the vicinity of polar TDI segments and those in the bulk layer are incorporated near less polar PPO segments. Although the local concentration of pyrene in the surface layer is higher than that in the bulk layer, the excimer formation is less feasible in the surface layer than in the bulk layer, due to the formation of nonemissive ground-state pyrene dimer in the surface layer.

Introduction

Surfaces and interfaces of polymer systems have received a lot of attention, because of their characteristic properties, functions, and many technological needs for surface modification for biocompatibility, adhesion, and surface treatment for resist materials in a semiconductor process. Adhesive or repulsive interactions at a surface or interface change conformation, orientation, and mutual association of a polymer from those of the bulk. These arrangements of a polymer chain effect the distribution of free volume and local concentration of a dopant or impurity. These surface effects sometime extended from 10 to 100 nm,

0897-4756/91/2803-0413$02.50/0